A Mechanism for Observed Interannual Variabilities over the Equatorial Indian Ocean

PRASHANT GOSWAMI AND NANDINI HARINATH

Council of Scientific and Industrial Research Centre for Mathematical Modelling and Computer Simulation, Bangalore, India

(Manuscript received 14 July 1995, in final form 14 October 1996)

ABSTRACT

A mechanism is proposed that can give rise to a sustained interannual variability of sea surface temperature (SST) and other variables even over an ocean basin of small zonal extent such as the Indian Ocean, as observed. A simple one-dimensional ocean–atmosphere coupled climate model with ''minimal'' dynamics is considered to isolate and emphasize the basic physical mechanism. In particular, unlike in the conventional scenario of the El Niño–Southern Oscillation, the equatorial Rossby waves are not included in the dynamics of the model. However, although the dynamics is minimal, the model as a whole is nonlinear due to the nonlinear parameterization of the atmospheric heating. It is shown that even with this minimal dynamics the model exhibits interannual variabilities for appropriate air–sea interaction. Further, in the one-dimensional case a basic factor that suppresses variability over the smaller basins is the zonal extent of the ocean basin. For an ocean-covered globe and for two basins of equal size separated by a land strip, the model shows interannual variability of about 5-yr period over both the eastern and the western sector (or basins). For two unequal ocean basins, with zonal extents representative of the Indian Ocean and the Pacific Ocean, only the larger basin shows sustained interannual oscillations. However, the observed interannual viability over the smaller (Indian Ocean) basin can be recovered if evaporation–wind feedback is included in the modeling of air–sea interaction. The phase relationship of the two oscillations, on the other hand, is affected by both basin geometry and moist feedback. Thus, it is proposed that both basin geometry and ocean–atmosphere coupling in the presence of moist feedbacks are essential to account for the observed structure and distribution of interannual variabilities in the Tropics.

1. Introduction

One of the most prominent variabilities in the Tropics is the El Niño–Southern Oscillation (ENSO). Following the conceptualization of ENSO as a manifestation of ocean–atmosphere interaction by Bjerknes (1969), a large number of analytical and modeling studies have focused on developing a dynamical scenario for ENSO phenomena involving air–sea interaction. However, in light of recent more detailed analysis of observational data, it appears that the current generally accepted dynamical scenario for ENSO variabilities may not be able to explain all its characteristics.

The present dynamical scenario of El Niño assumes that it is an event limited to the Pacific Ocean, although the atmospheric component of ENSO variability is global in character. In the conventional explanation of El Niño, this can be understood as a manifestation of the delayed oscillator mechanism (Cane and Zebiak 1985; Suarez and Schopf 1988; Battisti and Hirst 1989; Philander 1992) in which oceanic wave dynamics and the reflection of these waves determine the structure and growth of coupled instability. The local instability or growth rate of SST in this model is controlled by both local dynamical processes and remote processes due to wave dynamics. The local processes that mainly contribute are horizontal advection, anomaly upwelling, vertical thermal structure of the ocean, and heat flux to the atmosphere. In the remote processes the Rossby waves generated by wind stress anomalies propagate west and reflect off the western boundary and generate Kelvin waves. Because of the crucial role of the remote forcing, an important requirement of such a scenario is a critical size of the ocean basin (for particular phase speeds of the waves); thus in this scenario ocean basins with zonal extent much smaller than 13 000 km cannot support ENSO-type interannual variabilities (Battisti and Hirst 1989). This finding has been used to argue that ENSO-type interannual variabilities should be absent over the tropical Atlantic and the Indian Ocean (Battisti and Hirst 1989). Furthermore equatorial Rossby waves and hence meridional dynamics are essential components of this scenario. A delayed-oscillator-type mechanism as outlined above cannot be operative either for an ocean basin of small zonal extent or in the absence of meridional dynamics.

However, contrary to earlier belief, several recent observational studies suggest that ENSO-related variabilities are also present outside the tropical Pacific. A global relation of the surface pressure anomalies to the

Corresponding author address: Dr. Prashant Goswami, C-MMACS, Bangalore, 560 037 India.
E-mail: goswami@cmmacs.ernet.in

ENSO cycles was demonstrated by Krishnamurti et al. (1986). These results also conform to earlier studies made by Barnett (1985), who presented evidence of eastward propagation of surface winds and pressure anomalies from the equatorial Indian Ocean toward the central Pacific. Yasunari (1987), using an objectively analyzed time-filtered dataset for variables like SST, sea level pressure, and wind over the entire globe during El Niño episodes for the period 1964–1985, showed that positive SST anomalies appear both over the equatorial Indian Ocean and Atlantic Ocean almost in phase with the warm episode over the eastern Pacific. It was thus suggested by Yasunari (1987) that ENSO should be considered as a global phenomenon in a land–atmosphere–ocean coupled environment. A detailed analysis of the structure of the interannual variabilities in the atmospheric and oceanic variables over the tropical Pacific and the Indian Ocean was carried out by Nigam and Shen (1993). Their analysis of Comprehensive Ocean–Atmosphere Data Set (COADS) observations once again showed the presence of positive SST anomalies over the tropical Indian Ocean during El Niño periods. Several other studies also indicate that the ENSO type variabilities in SST are seen over the global ocean. Tourre and White (1995) report an analysis of 13 years (1979–1991) of data of spatiotemporal evolution of the ENSO signal in SST along with other variables for the Pacific, Indian, and Atlantic Oceans, that shows dominant EOF modes for SST associated with ENSO for both the Pacific and the Indian Ocean. The aim of the present study is to explore mechanisms that can support interannual variabilities on ocean basins of zonal extent much smaller than that required by the delayed oscillator mechanism and comparable to that of the Indian Ocean.

It should be noted that the amplitudes of the variabilities over the Indian Ocean are much smaller than those over the Pacific in general (Yasunari 1987; Nigam and Shen 1993). Thus, observationally, there is an asymmetry between the larger (Pacific) and the smaller (Indian) ocean basins in terms of the characteristics of interannual variabilities (such as amplitude). Therefore we expect that the basin geometry does play a crucial role in the evolution and structure of the interannual variabilities. In addition, we also envisage that improvement of the parameterization of air–sea interaction is necessary and crucial to simulate the observed variabilities in the Tropics. Thus, our philosophy in this work will be to explore a model with minimal dynamics with emphasis on air–sea interaction and land–ocean distribution. The importance of basin configuration and the presence of land in the dynamics of the coupled ocean–atmosphere system was demonstrated by Anderson and McCreary (1985, hereafter AM) using a simple coupled model with two ocean basins. The basin geometry was chosen to mimic the Indian Ocean and the Pacific basin configuration, with the ''Indian Ocean'' basin having a much smaller zonal extent (~7500 km) than that of the ''Pacific'' basin (~15 000 km). For the two independent ocean basins of equal size (15 000 km) with a dividing line of land, the two ocean basins, although physically separated, get dynamically connected. A region of warm temperature develops in one ocean and propagates eastward. This disturbance on reaching the eastern boundary affects the second ocean basin, which then propagates eastward. In the presence of land, and for one basin about half the size of the second basin (15 000 km), however, the equatorial SST in the smaller basin gets locked into a steady state (weakly warm and nonoscillatory), while the larger ''Pacific'' ocean exhibits low-frequency oscillations with a period of about 5 years. However, as we have emphasized earlier, although the ENSO signal is the strongest over the tropical Pacific, these variabilities are more global in character.

Even a very simple model with minimal dynamics can support interannual oscillations in a coupled system. Lau (1981, hereafter L81) considered a one-dimensional coupled model with only zonal dynamics for the equatorial climate system to simulate oscillations with interannual timescales. This points to the possibility that it is the air–sea coupling rather than detailed dynamics that play a more important role in the dynamics of the interannual variabilities. Furthermore, the study of AM also shows that the basin geometry and the presence of land significantly modulate the nature and structure of the coupled oscillation. However, most of the studies mentioned above do not include moist processes in the formulation of air–sea interaction. We anticipate and show that inclusion of moist feedback, namely, evaporation–wind feedback (hereafter EWF) in air–sea coupling in the presence of land can give rise to interannual oscillation also in a small ocean basin, although with reduced amplitude. We demonstrate this by using a model that has a minimal dynamics, namely, a one-dimensional model with only zonal dynamics. This implies that meridional dynamics and hence the Rossby wave dynamics are absent in our model. Our basic equations as well as the parameterization schemes for atmospheric heating and EWF are described in section 2. Section 3 contains a description of the results. In section 4 we provide a discussion of the results and advance our major conclusions.

2. The basic model

In accordance with our philosophy outlined above, we consider a model that describes the one-dimensional zonal dynamics of a coupled ocean–atmosphere system. In addition, we neglect the nonlinear advective terms in atmospheric and oceanic dynamics. However, the model as a whole is nonlinear because of the nonlinear parameterization of atmospheric heating. This is in line with our central hypothesis that it is the air–sea interaction and basin configuration that play a crucial role in the genesis and observed structure of interannual variabilities. The equations governing the atmospheric and

TABLE 1. Description of important model parameters.

Description of parameters	Notation	Typical values
Damping coeff. for the atmosphere	D_a	2.5×10^{-7} s^{-1}
Damping coeff. for the ocean	D_o	2.2×10^{-8} s^{-1}
Phase speed of the atmos. wave	c_a	15.0 m s^{-1}
Phase speed of the oceanic wave	c_o	2.0 m s^{-1}
Heating coefficient	ε	3.0×10^{-5} m s^{-2}
Evaporation wind feedback coeff.	Λ	1.0×10^{-5} m s^{-2}
Coeff. for ocean–atmospheric coupling	σ	1.91×10^{-4} s^{-1}
Wind stress	γ	2.16×10^{-8} s^{-1}
Upwelling	B	0.03 °C m^{-1}
Damping coeff. for SST	D_n	0.5×10^{-7} s^{-1}
Mean zonal SST gradient	$d\bar{T}/dx$	6.0×10^{-6} °C m^{-1}

the oceanic variables for the coupled system can be written as

$$\frac{\partial u_a}{\partial t} + \frac{\partial \phi}{\partial x} + D_a u_a = 0 \tag{1}$$

$$\frac{\partial \phi}{\partial t} + c_a^2 \frac{\partial u_a}{\partial x} + D_a \phi - \sigma\eta = Q_c \tag{2}$$

$$\frac{\partial u_o}{\partial t} + \frac{\partial \eta}{\partial x} + D_o u_a + \gamma u_a = 0 \tag{3}$$

$$\frac{\partial \eta}{\partial t} + c_o^2 \frac{\partial u_o}{\partial x} + D_o \eta = 0, \tag{4}$$

where the subscripts a and o refer to atmospheric and oceanic variables respectively, u is the zonal velocity component; ϕ and η are the geopotential and thermocline depth respectively, D is the damping coefficient, γ and σ are the coupling coefficients for the ocean by wind stress; and the term $\sigma\eta$ represents the effect of oceanic dynamics on atmospheric thermodynamics (L81). A description of the basic parameters and their typical values are provided in Table 1.

Our basic equations as well as notations and conventions are very similar to those of L81. However, unlike L81, we do not interpret the dynamics in terms of equatorial Kelvin waves. For one thing, unlike the case of equatorial Kelvin dynamics, the zonal velocity component in the present case cannot be in geostrophic balance. Since there is no meridional pressure gradient, the dynamics does not include any β effect and hence the eigenfunctions cannot exhibit the characteristic β dependence for Kelvin wave eigenfunction. We should therefore like to interpret our model as a minimal model describing the zonal dynamics of the coupled system. In addition to governing equations (1)–(4), we also include an equation describing the dynamics of sea surface temperature, T:

$$\frac{\partial T}{\partial t} - u_o \frac{\partial \bar{T}}{\partial x} - B\frac{\partial \eta}{\partial t} + D_n T = 0. \tag{5}$$

This equation for SST is similar to one used in many studies of coupled dynamics (e.g., Lau and Shen 1988). The parameters B and D_n are as given in Table 1. Here $\bar{T}$ is the mean value of SST.

a. Parameterization of atmospheric heating and evaporation–wind feedback

The atmospheric heating term Q_c is expressed as a function of divergence of u_a:

$$Q_c = \begin{cases} \varepsilon\delta_i, & \delta_i > 0 \\ 0, & \delta_i < 0, \end{cases}$$

$$\delta_i = u_{a,i+1} - u_{a,i}, \tag{6}$$

where i is zonal index. The term Q_c parameterizes atmospheric heating due to convection in the Tropics. This parameterization is identical to the one adopted in L81 and provides a rough measure of the upper-level divergence between adjacent zonal domains. The scaling parameter ε can be visualized as an efficiency factor of the convective processes in the atmospheric heating and is assigned a value of 3×10^{-5} m s^{-2} (Table 1) following L81. In addition, we also include the effects due to moist feedbacks, namely, EWF, by using the bulk aerodynamic formula as follows:

$$E = \begin{cases} 0 & \text{over land} \\ \rho_a C_D \Delta q_s |u_a| & \text{over ocean,} \end{cases} \tag{7}$$

where Δq_s is the mean humidity difference between the sea surface and anemometer level. In the presence of EWF the atmospheric heating is modified and is given by the balance equation between column convergence of moisture, total column precipitation, and gain of moisture due to evaporation from the lower boundary. This balance can be expressed as

$$-H\frac{d\bar{q}}{dz}\frac{\partial u_a}{\partial x} = E - P, \tag{8}$$

where H is the height of the (lower tropospheric) atmospheric column and P is the precipitation in kilograms per unit area per unit time. Since the effect due to the convergence is already included in the term Q_c, we neglect the convergence term in the above equation and write an expression for the heating component due to EWF as

$$Q_{\text{ewf}} = \frac{L_v}{C_p H} C_D \Delta q_s |u_a| = \Lambda |u_a|, \tag{9}$$

where L_v is the latent heat of precipitation. With typical values of drag coefficient $C_D = 1.0 \times 10^{-3}$, $\Delta q_s = 1\%$–5%, and $H = 5000$ m, Λ is of the order 10^{-5}. We shall consider a typical value of $\Lambda = 1.0 \times 10^{-5}$. It should be noted that due to the adopted parameterization of atmospheric heating, Q_c and EWF, our model is essentially nonlinear. The parameterization of EWF adopted here has been used by several authors in a linearized form in the investigation of low-frequency variabilities in the Tropics (Neelin et al. 1987; Lau and Shen 1988; Goswami and Goswami 1991). In the linearized version of the parameterization of EWF, a heating anomaly in the Tropics characterized by mean background easterly

winds gives rise to an enhancement of the winds and hence EWF in the eastern sector and a lowering of convective heating in the western sector. Such a scenario still holds for the present case, although unlike the analytical studies, in the parameterization adopted here EWF is proportional only to the wind speed.

b. Basin configuration and parameterization of land

The primary effect of land in our model is to introduce a discontinuity in the spatial distribution of the oceanic variables. This formalism is therefore similar to that of AM. In our formalism, however, there is another effect that distinguishes between the land and the ocean: This is the process of EWF; in the simplest case considered here, which may be called dry land approximation, the difference between humidity values at the surface and the anemometer level is zero over land. Over the ocean the EWF is determined by bulk aerodynamic formula [Eq. (7)]. Thus the presence of land can affect the coupled dynamics both mechanically and thermodynamically. As we shall see, this has a major effect. As in AM, the presence of land is parameterized by setting the oceanic variables to zero over land. In addition, the oceanic variables are required to satisfy boundary conditions in the eastern and the western boundaries. The atmospheric wind is required to be continuous across the boundaries by requiring

$$u_a(\text{ocean}) = u_a(\text{land})$$

$$\frac{\delta u_a(\text{ocean})}{\delta x} = \frac{\delta u_a(\text{land})}{\delta x}$$

at the land–ocean boundaries.

On the lateral boundaries of the x domain we take the u_a and u_o to be zero and mean easterly winds of 3 m s^{-1} are assumed over the whole domain. The zonal domain has been divided into 9 strips, each measuring 35°. In the all-ocean case, all nine strips represent ocean. In the equal basin case (hereafter EOB), the first three strips represent ocean, the next three land, and the last three again ocean. In the unequal ocean basin case (hereafter UOB), the first two strips represent ocean, the next two strips land, and the last five strips ocean. The momentum equations in (1)–(4) are averaged over each strip and the spatial derivatives in (2) and (4) are expressed in terms of the strip-averaged quantities. The two land–ocean configurations considered here are presented schematically below.

c. Schematic diagram of the basin configuration

(i) Equal ocean basin (EOB):

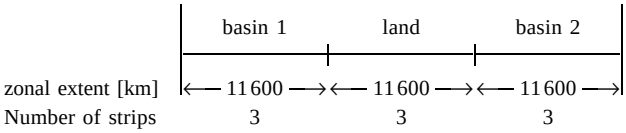

(ii) Unequal ocean basin (UOB):

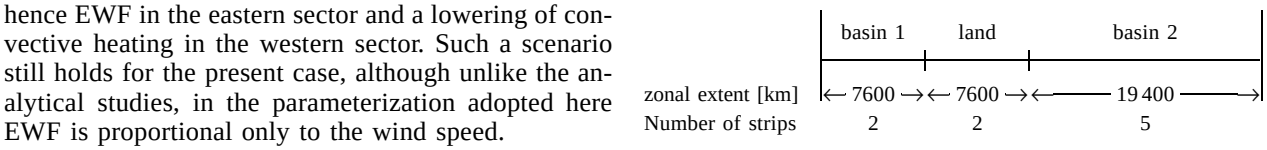

For each of the three configurations the model was then integrated for about 60 years of model time with the given initial condition. While an identical value of time step $\delta t = 9.5 \times 10^3$ s was used for both the atmospheric and the oceanic component, the oceanic component was called for every fifth time step of model integration. In the following, the results are presented for a period of 20 years from 40 to 60 years of model integration.

3. Results

a. Interannual variability

Figures 1, 2, and 3 present longitude–time sections for zonal wind u_a (top panels) and SST (bottom panels) for the all-ocean case, EOB, and UOB respectively. The left panels show the results with zero EWF and the right panels with a nonzero EWF ($\Lambda = 1.0 \times 10^{-5}$) in all the figures. Interannual oscillation of a period of about 5 years is present for each variable in all the cases except for the bottom left panel of Fig. 3, which represents the time–longitude structure of SST for the smaller basin in the absence of EWF. A clear westward phase propagation is also evident in each case. Furthermore, from a comparison of the top and the bottom panels it can be seen that the zonal wind is ahead of the SST in phase in basin 2. The corresponding results in the presence of EWF shows that EWF does not affect the phase propagation characteristics significantly. It is now recognized that interaction between the ocean and the atmosphere can excite more than one unstable mode and there are at least two distinct types of unstable waves. One of these two unstable waves is characterized by a westward phase propagation such that at a fixed point the zonal winds lead the SST anomalies in phase. The ocean responds to the winds through an induced divergence field, with convergence and a deepened thermocline (higher SST) along the equator (Philander 1992). As can be seen from the results presented in Fig. 5 our findings can be explained through such a mechanism.

b. Interannual variability in the Indian Ocean basin

As shown in AM, when there are two ocean basins of unequal size, with the smaller ocean basin separated from the larger eastern basin by a land strip; the interannual variabilities for the two basins are different. This is also true in the present case, and in the absence of EWF no sustained oscillation of appreciable amplitude takes place in the smaller ocean basin. Thus the AM

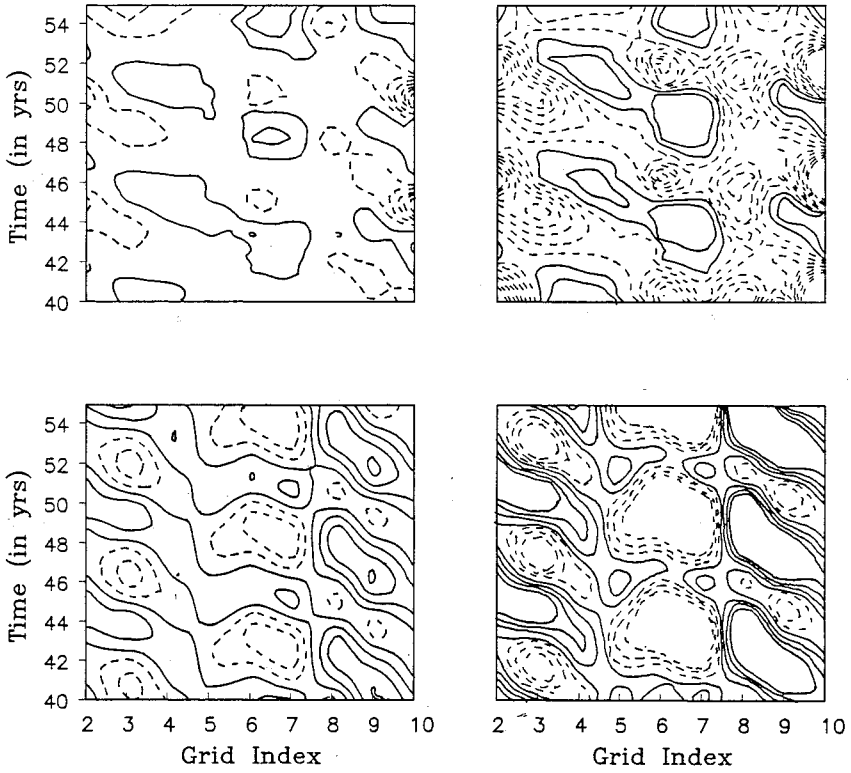

FIG. 1. Longitude–time plot of the wind field (u_a) (top panels) and SST (bottom panels) for the all-ocean case. The left panels show the results in the absence of evaporation wind feedback, while the right panels show the results for a nonzero EWF (Λ). The x axis shows the zonal grid index, while the y axis shows time in years. Negative contours are dashed. Contours are u_a:min = −0.04, max = 0.01, contour interval = 0.005; SST:min = −0.12, max = 0.13, contour interval = 0.04. The minimum and maximum values referred to here are cutoff values.

model, and our model without EWF, fail to reproduce the observed El Niño-type variability in the Indian Ocean region (Yasunari 1987). However, the present model with the inclusion of EWF in the parameterization of air–sea interaction can give rise to the desired result. Inclusion of EWF not only produces a sustained oscillation over the smaller ocean basin, but also influences the phase of the variabilities.

These results are summarized in Figs. 4 and 5. Figure 4 shows the time evolution of the strip-averaged SST for the two basins (or two sectors), for the all-ocean case (top panels), EOB (middle panels), and UOB (bottom panels). The left panels show domain-averaged SST (K) for the western basin (or sector) and the right panels show domain-averaged SST for the eastern basin (or sector). In addition, for each basin configuration results are shown for two strengths of EWF: no EWF ($\Lambda = 0$, solid line) and moderate EWF ($\Lambda = 1.0 \times 10^{-5}$, dashed line). As can be seen from the top panels, EWF has the same effect on the amplitudes of the perturbations in both the sectors in the all-ocean case. Although there is a weak growth of the amplitude in the presence of EWF, the amplitudes do not exceed 1.4°C in sector 1 and stay very close to 1.4°C in sector 2, even after 60 years of model integration. It should be noted that an inherent asymmetry exists between the two sectors; the amplitude of the cold state (negative amplitude) in sector 2 is much smaller than that in sector 1. EWF has a profound effect on the amplitudes of the perturbations when two ocean basins of equal size are separated by a land region (middle panels). In basin 1, the amplitudes are small (~2.0°C) and are preferentially on the positive side for EWF = 0.0, but there is a greater tendency to oscillate between the warm (positive) and cold (negative) states. For a nonzero EWF, the amplitude is still close to 1°C. This scenario is nearly the same for the eastern ocean basin (middle, right panel); here the highest amplitudes (>8°C) are attained for EWF = 0.0, while for a nonzero EWF the amplitudes are comparable and are about 3°C. The scenario changes dramatically when the two basins are of unequal size, as shown in the bottom panels. Here basin 1 has a zonal extent of about 7700 km, separated from the larger basin (of zonal extent 19 400 km) by a land strip of 7700 km zonal extent. The configuration is adopted, as in AM, to represent the configuration of the Indian Ocean and the Pacific Ocean separated by a continental land mass. For this case, the smaller basin shows a nearly stable (weakly warm, amplitude ~0.1°C) state in the absence of EWF. For the same case, the larger ocean basin shows

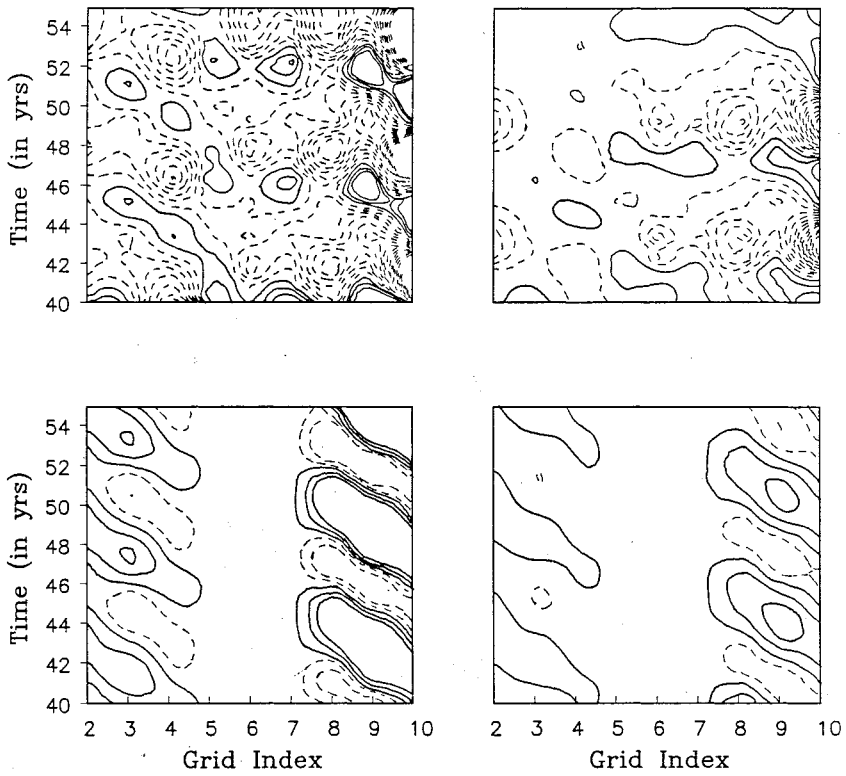

FIG. 2. Longitude–time plot of the wind field (u_a) (top panels) and SST (bottom panels) for the equal ocean basin case (EOB). The left panels show the results in the absence of evaporation wind feedback, while the right panels show the results for a nonzero EWF ($\Lambda = 1.0 \times 10^{-5}$). The x axis shows the zonal grid index, while the y axis shows time in years. Negative contours are dashed. Contours are u_a:min = -0.4, max = 0.08, contour interval = 0.01; SST:min = -0.12, max = 0.13, contour interval = 0.04. The minimum and maximum values referred to here are cutoff values.

oscillation with amplitudes of about 3°C. For the large ocean basin, EWF has no appreciable effect on the amplitudes; there is only a moderate enhancement from zero EWF (solid line) to nonzero EWF (dashed line). In contrast, the effect of EWF on the oscillations in the smaller basin is significant, with amplitude increasing about sixfold from 0.1 for no EWF to 0.6 for nonzero EWF. It should be noted that the oscillations in basin 1 are essentially on the positive side.

The phase relationships between the oscillations in the two basins are presented in Fig. 5. The top two panels show the relationship between SST for sector 1 (solid line) and sector 2 (dashed line) for the all-ocean case. The phase relationship between the SST fields of basin 1 (solid line) and basin 2 (dashed line) for the EOB and the UOB cases are presented in the middle and the bottom panels respectively. In each of these figures the left panels represent zero EWF and the right panels nonzero EWF ($\Lambda = 1.0 \times 10^{-5}$). In the all-ocean case (top panels) EWF reverses the phase relationship between the two basins, whereas in the EOB case (middle panels) EWF does not make a significant change in the phase relationship between the two basins. UOB with EWF (bottom right panel) clearly shows the in-phase relationship between basin 1 and basin 2. This in-phase relationship is more clearly brought about in the presence of EWF than in the absence of it.

c. Dynamical mechanism

To gain further insight into the mechanism of interannual oscillation in the present model, an analysis of the atmospheric heating field (longitude–time sections) with and without EWF is presented in Fig. 6. Once again, a uniform contour interval is adopted for each panel for advantage in interpretation. The left panels represent results in the absence of EWF, while those on the right represent the heating field in the presence of EWF ($\Lambda = 1.0 \times 10^{-5}$). The top, middle, and bottom panels represent the results for the three configurations: all-ocean, EOB, and UOB respectively. The first noticeable effect of EWF on atmospheric heating, as can be seen from the middle panels, is suppression of atmospheric heating for the EOB in the presence of EWF. On the other hand, for the UOB case EWF enhances the atmospheric heating even over the smaller basin (bottom right panel). This can be contrasted with the result presented in the bottom left panel for the zero

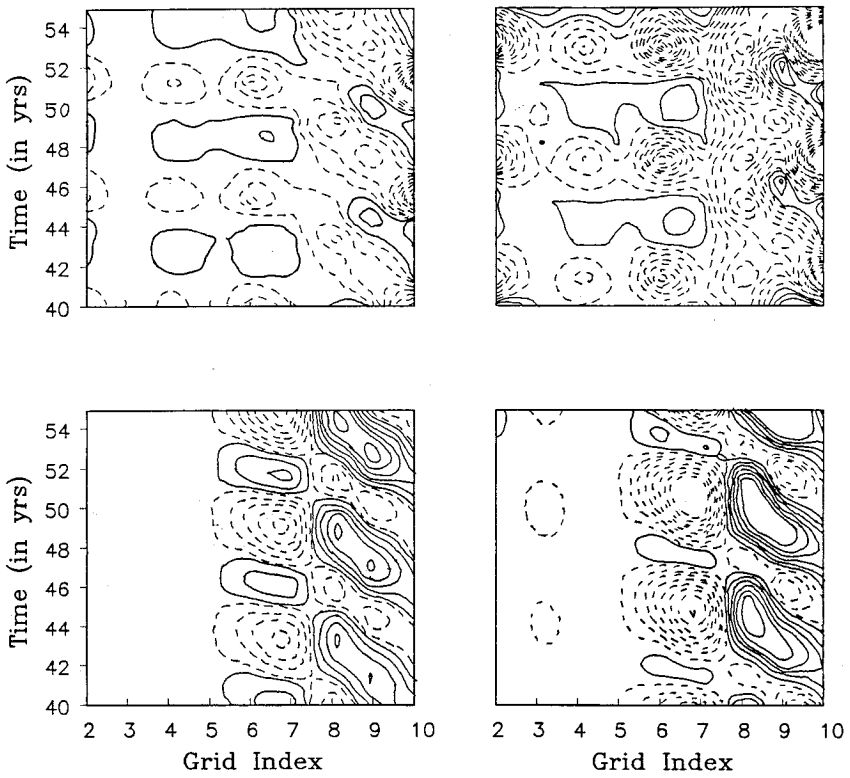

FIG. 3. Longitude–time plot of the wind field (u_o) (top panels) and SST (bottom panels) for the unequal ocean basin case (UOB). The left panels show the results in the absence of evaporation wind feedback, while the right panels show the results for a nonzero EWF ($\Lambda = 1.0 \times 10^{-5}$). The x axis shows the zonal grid index, while the y axis shows time in years. Negative contours are dashed. Contours are u_o:min = -0.12, max = 0.04, contour interval = 0.015; SST:min = -1.8, max = 0.9, contour interval = 0.15. The minimum and maximum values referred to here are cutoff values.

EWF, which shows no appreciable heating over the smaller basin.

The distribution of the oceanic divergence field for each of the basin configurations is presented in Fig. 7. The top, middle, and bottom panels represent the longitude–time sections for D_o in units of 10^{10} s^{-1} for the all-ocean, EOB, and UOB case respectively. The left panels show the results in the absence of EWF, while the right panels show the results in the presence of EWF ($\Lambda = 1.0 \times 10^{-5}$). The important effect of EWF on D_o is in terms of its strength. For the UOB case, with zero EWF (Fig. 7, bottom left panel), the maximum values for divergence ($D_o > 0$) and convergence ($D_o < 0$) are 100 and -80, respectively. For the UOB case with EWF nonzero (Fig. 7, bottom right panel), on the other hand, the maximum values of divergence and convergence are 220 and -110 respectively. Furthermore, for nonzero EWF, there is a substantial convergence field ($D_o < 0$) in the smaller basin. Thus the presence of EWF helps to generate downwelling (higher SST) in the smaller basin as seen from Fig. 7 (bottom right panel).

It is revealing to examine the phase relationship between SST (from Figs. 1, 2, and 3) and atmospheric heating (Fig. 6). Since the atmospheric heating in our model is essentially convective, the distribution of the heating field in Fig. 6 is a good indication of convective activity in our model. From a comparison of the lower panels of Fig. 1 (SST for the all-ocean case) with the top panels of Fig. 6 (atmospheric heating for the all-ocean case), we can see that positive SST anomaly nearly coincides with the maximum heating (high convection), both in the absence of EWF (left panels) and for nonzero EWF (right panels). The corresponding results for the EOB case can be obtained from the comparison of the lower panels of Fig. 2 with the middle panels of Fig. 6. An out-of-phase relationship between SST and atmospheric convection is most prominent for the UOB case (Fig. 3 and 6, bottom panels), especially for nonzero EWF. Such an out-of-phase relationship between the recurrent SST anomalies and the outgoing longwave radiation (OLR), which can be considered as a measure of intensity of convection, was demonstrated by Nigam and Shen (1993) over most of the tropical Pacific and Indian Ocean basins.

4. Conclusions

The present study shows that even a minimal model with only zonal dynamics can sustain interannual modes

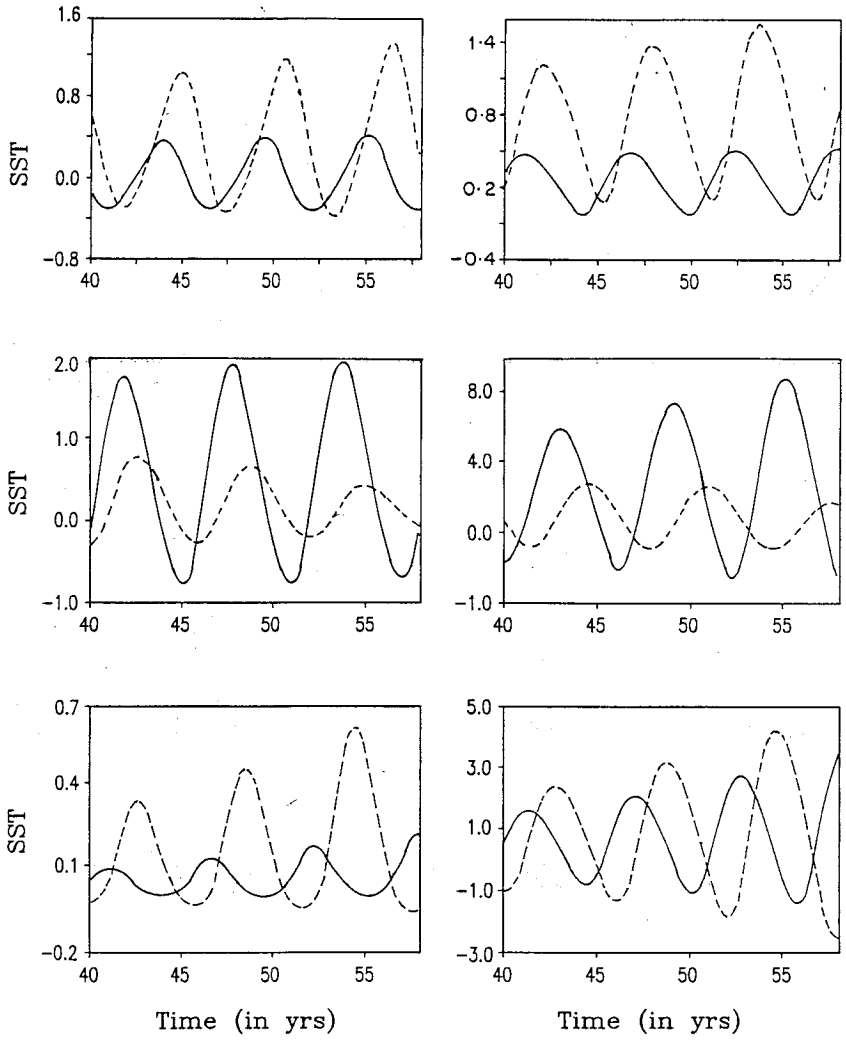

FIG. 4. Time series of basin-averaged sea surface temperature field for an all-ocean case (top panel), EOB case (middle panels), and UOB case (bottom panels). In each of these panels, the solid line represents zero EWF, while the dashed line represents the presence of a nonzero EWF ($\Lambda = 1.0\text{E}-05$). In each of these pairs, the left panels represent basin 1 and right panels basin 2.

in an ocean–atmosphere coupled environment. This was also found in Lau (1981) for an all-ocean case using a simple one-dimensional coupled model for the equatorial region. In the present case we have also included the presence of land and evaporation–wind feedback. The land–ocean configuration adopted in our model is similar to that considered in AM. As shown in AM, which considered a two-dimensional model but no EWF, when the two ocean basins are of unequal size, separated by a land region of size comparable to that of the smaller ocean basin, no oscillation evolves over the smaller ocean basin. This is also seen in the present case, in spite of the fact that the dynamical effects due to the motion in the meridional direction are not present in our model. However, this scenario is significantly changed in the presence of EWF. Although EWF does not affect the amplitudes of oscillation significantly over the larger ocean basin, the smaller ocean basin, which exhibits a nearly steady (weakly warm) state in the absence of EWF, supports an oscillation of amplitude about 0.6.° in the presence of a moderate EWF. These oscillations are in phase with the warm episodes of the larger basin. As we have mentioned earlier, this situation is very similar to the one found observationally (Yasunari 1987; Nigam and Shen 1993). It is therefore proposed that moist feedbacks, especially EWF, along with unequal basin configuration provide a basic mechanism for the observed interannual variability over the Indian ocean region, occurring in phase with the El Niño episodes over the Pacific (Yasunari 1987).

The importance of moist feedback, in particular the effect of surface heat flux anomalies on the modes of

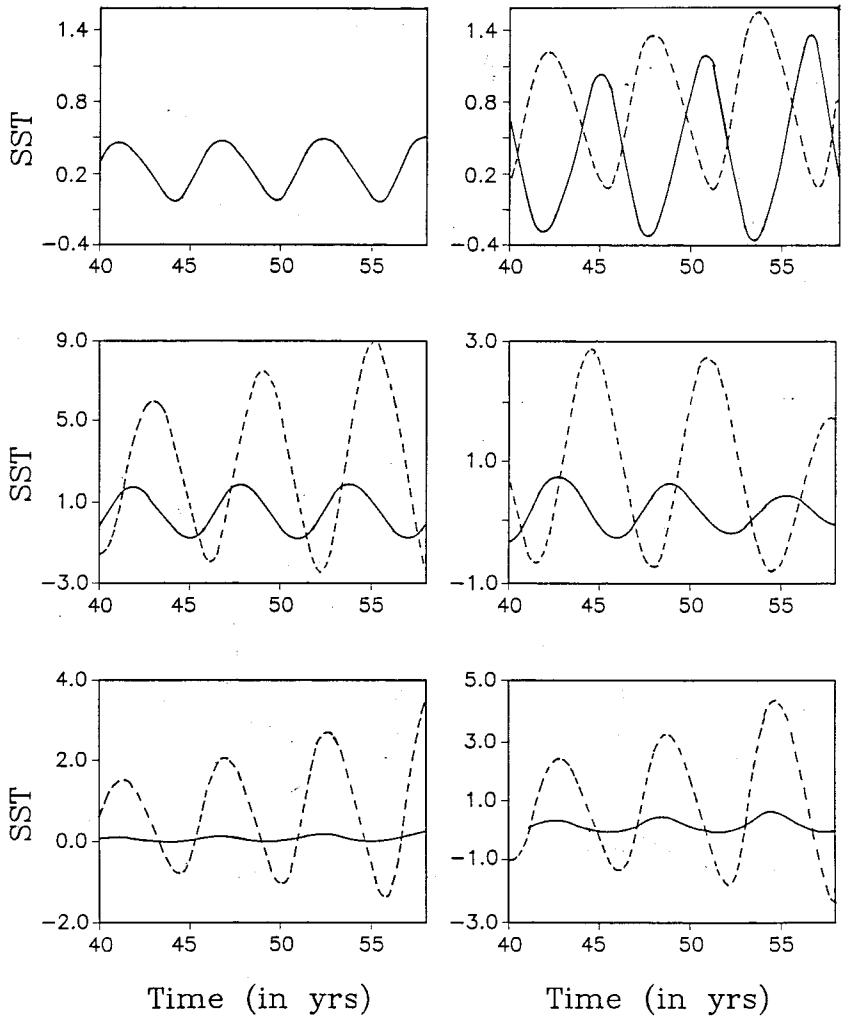

FIG. 5. Phase relationship between the basin-averaged SSTs for the two basins (or sectors for the all-ocean case) for the all-ocean (top panels), EOB (middle panels), and UOB (bottom panels) cases. The solid line represents basin 1 and the dashed line represents basin 2. In each of these panels, the left panels represent the case of zero EWF, while the right panels show results with a nonzero EWF ($\Lambda = 1.0\text{E}-05$).

tropical coupled variabilities, was reported by Miller and Jiang (1995). Using a 100-year simulation by coupled ocean–atmosphere GCM (CGCM), they showed that the EWF can lead to mode growth both in presence of mean easterlies and mean westerlies, as over the Indian Ocean. The SST budget from their 100-year model run shows that modes of variability originate from surface heat fluxes and reduced upwelling. The results from our extremely simple coupled model are very similar to the results of Miller and Jiang (1995) obtained using the simulation of a CGCM. This points to the possibility that moist feedback and basin configuration play crucial roles in simulation of the observed variabilities.

Another important conclusion, which goes beyond the explanation of the observed structure of interannual variabilities over the Indian Ocean region, is that the delayed oscillator mechanism may not be necessary or even appropriate for understanding the genesis of interannual variabilities in the Tropics. Even the local dynamical processes like oceanic upwelling and atmospheric heating due to interaction between convection and large-scale dynamics can lead to sustained oscillations with characteristics very similar to those observed. The remote processes, due to wave reflection, appear to play only a secondary role in the genesis, although they may be important for the detailed spatial structure of the variabilities. The basic genesis mechanism, as can be seen from Figs. 6 and 7, involves variabilities with a westward, rather than eastward, propagation of phase. As we have mentioned earlier, the phase propagation characteristics of the atmospheric and the oceanic quantities are not the same. It has been known from stability analysis of the coupled ocean–atmosphere models that an unstable mode exists with

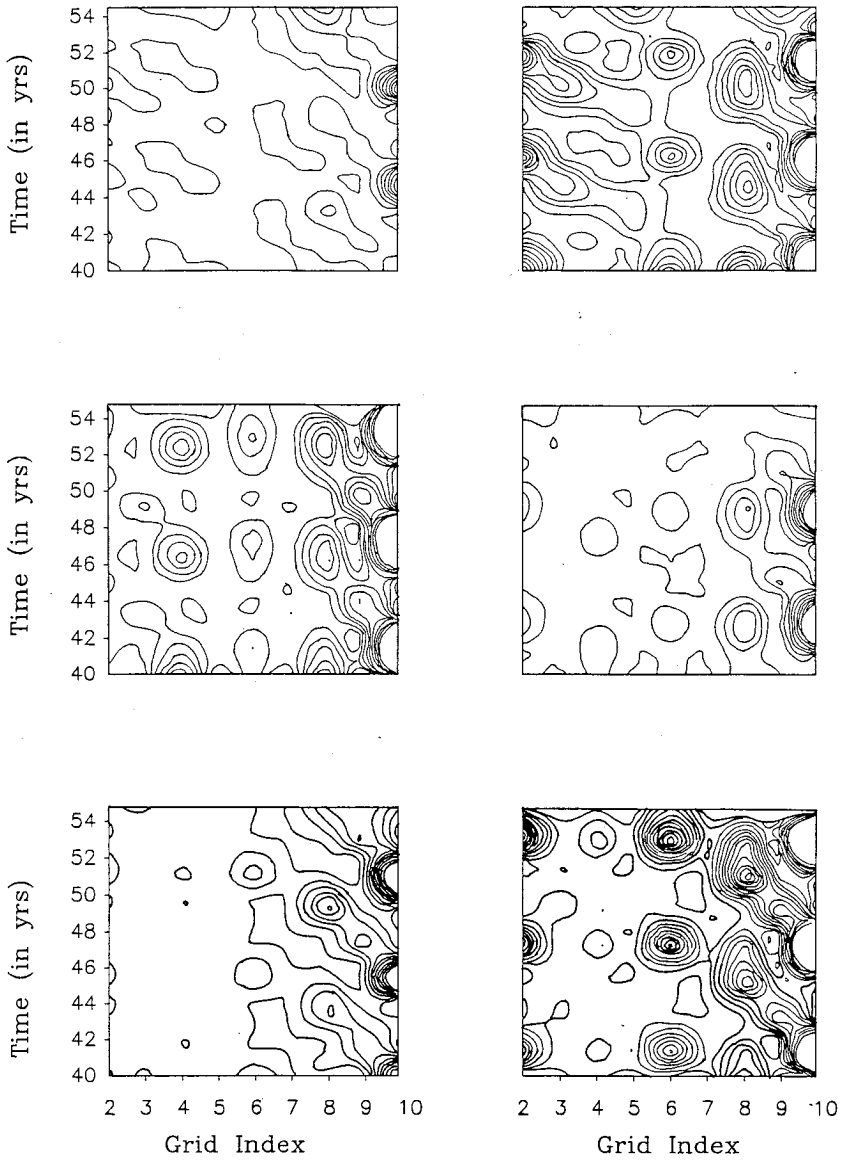

FIG. 6. Longitude–time plot of the atmospheric heating field ($q_i \times 10^6$) for three configurations: all-ocean (top panels), two equal basins (middle panels), and two unequal ocean basins (bottom panels). The left panels show the results in the absence of evaporation wind feedback, while the right panels show the results for a nonzero EWF ($\Lambda = 1.0 \times 10^{-5}$). The x axis shows the zonal grid index, while the y axis shows time in years. Contours are all-ocean: max = 2, contour interval = 0.2; EOB:max = 5, contour interval = 0.5; UOB: max = 6, contour interval = 0.5. The maximum values referred to here are cutoff values.

westward phase propagation. Such a mode seems to be associated with the seasonal cycle along the equator (Philander 1992; Horel 1982). The characteristics of this mode for a scenario in which the oceanic response to the wind forcing involves waves explicitly were studied by Hirst (1988). In another study, Neelin (1991) investigated the characteristics of the westward propagating wave for a case that does not involve waves explicitly. For this case neither waves nor coasts play any role in the genesis and the dynamics of the evolution. The dynamical mechanism involved (Philander 1992) includes westerly winds in response to a warm SST anomaly, induced convergent oceanic motion, downwelling, and associated increase in SST. The westward displacement of SST caused by the winds causes a farther westward displacement of the winds and a westward propagating disturbance results. From Figs. 6 and 7, a similar mechanism seems to be operative in the present case.

It remains to be seen if the basin asymmetry effect of EWF on the growth of instabilities found in our studies is supported by more detailed diagnostic studies. The period of oscillation of the coupled variability was found

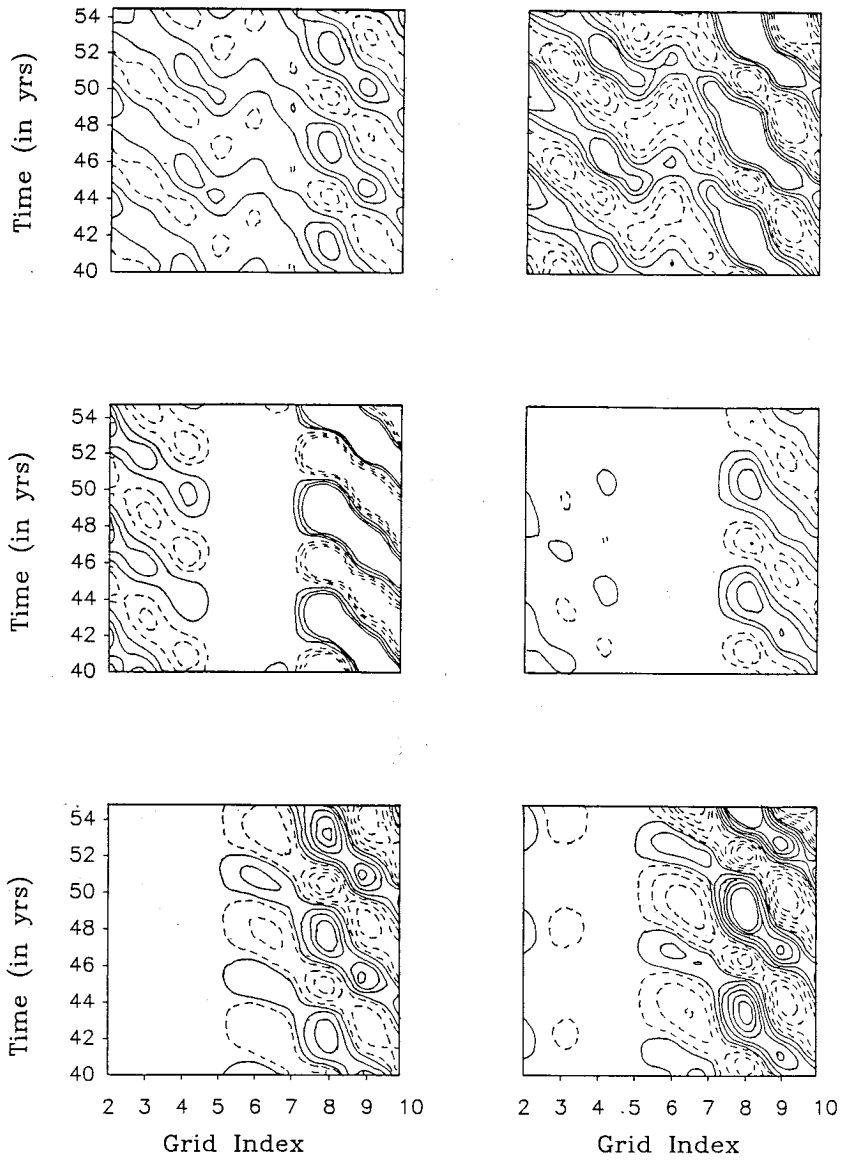

FIG. 7. Longitude–time plot of the oceanic divergence field ($D_o \times 10^{10}$ s^{-1}) for three configurations: all-ocean (top panels), two equal basins (middle panels), and two unequal ocean basins (bottom panels). The left panels show the results in the absence of evaporation wind feedback, while the right panels show the results for a nonzero EWF ($\Lambda = 1.0 \times 10^{-5}$). The *x* axis shows the zonal grid index, while the *y* axis shows time in years. Negative contours are dashed. Contours are all ocean: min = −15, max = 15, contour interval = 5; EOB: min = −40, max = 45, contour interval = 10; UOB: min = −80, max = 110, contour interval = 20. The minimum and maximum values referred to here are cutoff values.

sensitive to some model parameters, namely, the gravity wave speed C_a, which in turn depends on the assumed equivalent depth of the atmosphere. Such a sensitivity of the characteristics of the interannual variability to the equivalent depth of the atmosphere was also reported by Chang and Webster (1995). Using a coupled model like AM, they find that the strength, the periodicity, and even the existence of interannual variability depend on the value of the equivalent depth adopted for the atmosphere.

Another important issue in the formulation and performance of coupled models is the model numerics; either the westward propagating mode mentioned earlier or a delayed oscillator type mode may result depending on the resolutions of the components of the coupled model (Lau et al. 1992; Philander 1992). When the ocean has a coarse resolution, as in the present case, local processes like wind-induced upwelling govern the genesis and evolution of the variabilities and remote processes are not important. With higher resolution,

when the waves are adequately resolved, remote processes involving wave dynamics can give rise to a delayed oscillator type mode. Thus, conclusions of the present study may be modified. However, even if a high-resolution model with only zonal dynamics produces an interannual variability that involves remote processes, the inherent mechanism will have to be radically different from the current delayed oscillator mechanism that involves both Kelvin and Rossby waves. This point is currently under investigation.

Also, as can be seen from Figs. 4 and 5, there is a weak growth of amplitudes with time. This indicates the need for the inclusion of detailed nonlinear dynamics. Another important feature of ENSO variabilities, which the present model with its one-dimensional dynamics cannot explain, is the meridional structure of the anomalies. Besides, the oscillations in the present case are too periodic and do not show the characteristic irregularities of the observed ENSO variabilities. It is possible that once the ocean–atmosphere coupling generates the basic oscillation, normal modes will be excited both in the ocean and the atmosphere. In a two-dimensional case, these normal modes will involve equatorial Kelvin and Rossby waves, which in the larger ocean basin can give rise to the delayed oscillator mechanism in addition to the basic mechanism proposed here. These aspects need investigation with more complex models.

REFERENCES

Anderson, D. L. T., and J. P. McCreary, 1985: On the role of the Indian Ocean in a coupled ocean–atmosphere model of El Niño and the Southern Oscillation. *J. Atmos. Sci.,* **42,** 2439–2442.

Barnett, T. P., 1985: Variations in near-global sea level pressure. *J. Atmos. Sci.,* **42,** 478–501.

Battisti, D. S., and A. C. Hirst, 1989: Interannual variability in a tropical atmosphere–ocean model: Influence of the basic state, ocean geometry and nonlinearity. *J. Atmos. Sci.,* **46,** 1687–1712.

Bjerknes, J., 1969: Atmospheric teleconnections from the equatorial Pacific. *Mon. Wea. Rev.,* **97,** 163–172.

Cane, M. A., and S. E. Zebiak, 1985: A theory for El Niño and the Southern Oscillation. *Science,* **228,** 1084–1087.

Chang, H-R., and P. J. Webster, 1995: Studying the mechanisms of international variability with a coupled ocean–atmosphere model. *Extended Abstracts, TOGA 95 Int. Conf.,* Melbourne, Australia, TOGA, 147.

Goswami, P., and B. N. Goswami, 1991: Modification of n = 0 equatorial waves due to interaction between convection and dynamics. *J. Atmos. Sci.,* **48,** 2231–2244.

Hirst, A. C., 1988: Slow instabilities in tropical ocean basin–global atmospheric models. *J. Atmos. Sci.,* **45,** 830–852.

Horel, J. D., 1982: The annual cycle in the tropical Pacific atmosphere and ocean. *Mon. Wea. Rev.,* **110,** 1863–1878.

Krishnamurti, T. N., S. H. Chu, and W. Iglesian, 1986: On the sea level pressures of the Southern Oscillation. *Arch. Meteor. Geophys. Bioclimatol. Ser. A,* **34,** 385–425.

Lau, K. M., 1981: Oscillation in a simple equatorial climate system. *J. Atmos. Sci.,* **38,** 248–261.

——, and S. Shen, 1988: On the dynamics of intraseasonal oscillation and ENSO. *J. Atmos. Sci.,* **45,** 1781–1797.

Lau, N. C., S. G. H. Philander, and M. J. Nath, 1992: Simulation of low ENSO-like phenomena with a resolution coupled GCM of the global ocean and atmosphere. *J. Climate,* **5,** 284–307.

Miller, R. L., and X. J. Jiang, 1995: Surface heat fluxes and coupled variabilities in the Tropics of a coupled general circulation model. *Extended Abstracts, TOGA 95 Int. Conf.,* Melbourne, Australia, TOGA, 328.

Neelin, J. D., 1991: The slow sea surface temperature mode and the fast wave limit: Analytic theory for tropical interannual oscillations and experiments in a hybrid coupled model. *J. Atmos. Sci.,* **48,** 584–606.

——, and I. M. Held 1987: Modeling tropical convergence based on the moist static energy budget. *Mon. Wea. Rev.,* **115,** 3–12.

Nigam, S., and H. S. Shen, 1993: Structure of oceanic and atmospheric low frequency variability over the tropical Pacific and Indian Oceans. Part I: COADS observations. *J. Climate,* **6,** 657–677.

Philander, S. G. H., 1992: Ocean–atmosphere interaction in the tropics: A review of recent theories and models. *J. Appl. Meteor.,* **31,** 938–945.

Schopf, P. S., and M. J. Suarez, 1988: A delayed action oscillator for ENSO. *J. Atmos. Sci.,* **45,** 3283–3287.

Tourre, Y. M., and W. B. White, 1995: ENSO signals in global upper ocean temperatures. *Extended Abstracts, TOGA 95 Int. Conf.,* Melbourne, Australia, TOGA, 119–120.

Yasunari, T., 1987: Global structure of the El-Niño/Southern Oscillation. Part I: El-Niño composites. *J. Meteor. Soc. Japan,* **65,** 65–80.